JMEPEG (2024) 33:7040–7053
https://doi.org/10.1007/s11665-023-08462-8

1059-9495/$19.00

ORIGINAL RESEARCH ARTICLE

Properties of Porous Mullite Filter Material Fabricated from Reaction Sintered Mullite Grains

Nthabiseng Ntholeng, Patrick Rokebrand, Nthape Percyval Mphasha, and Iakovos Sigalas

Submitted: 13 September 2022 / Revised: 17 April 2023 / Accepted: 23 April 2023 / Published online: 5 July 2023

This research investigates the fabrication of porous mullite filter material from reaction sintered mullite grains for high-temperature applications. Current filter types are not suitable for application in high-temperature and corrosive environments despite their high porosity. Acicular Mullite Ceramics are known for their highly porous microstructures with excellent mechanical integrity. Fabrication of a rod-like porous mullite filter from mullite grains produced from pyrophyllite clay and Al_2O_3 via reaction sintering was investigated. Pure mullite phase was produced at 1600 °C, and the use of a binder and foaming agent helped to obtain a porous structure. Above 1700 °C, acicular mullite grain growth via two-dimensional heterogeneous nucleation was promoted. A friable and structurally poor material was produced at temperatures just below 1800 °C. Above 1800 °C, the structural integrity of the ceramic material was improved. The measured total porosity and average pore diameter at 1800 °C were 36.20% and 29.32 μm, respectively. The measured density was 1.99 g/cm^3, and the average compressive strength was 12.60 MPa. The characteristic strength was 14.49 MPa, with a Weibull modulus of 2.67.

Keywords mechanical properties, porosity, pyrophyllite, SEM, sintering

1. Introduction

Hot gas filtration is a sustainable technique that can reduce environmental pollution caused by greenhouse gases and particulate matter (PM) emissions (Ref 1). Hence, the strict implementation of environmental regulations is necessary to reduce the emission of greenhouse gases which release particulate matter that may negatively affect the human lungs (Ref 2-4). The excessive emission of PM, at high temperatures, is mainly generated from automobile exhaust, cement plant exhaust, biomass burning, and coal combustion (Ref 5, 6). Hot gas filtration has been shown to improve product quality, process efficiency, and economics, as well as reduce high PM and gas emissions (Ref 7). For example, using hot gas filtration in the coal gasification process instead of wet scrubbing increases efficiency by 3%. Hot gas filtration enables the use of particle-free, high-temperature gas in subsequent or coupled process steps (Ref 7). Further, hot gas filtration can also be used to recover materials such as catalysts or noble metals from circular movement (Ref 7). Porous ceramics are becoming increasingly popular for hot gas filtration due to their unique properties such as low thermal expansion, shock resistance, corrosion resistance, and high-temperature mechanical stability (Ref 8). Porous ceramics such as cordierite, mullite, alumina, and silicon carbide are the leading candidates for high-temperature ceramic filters (Ref 9).

Fibrous filters are unsuitable for applications in high-temperature and corrosive environments, despite their high porosity ($>$ 70%), as they are mainly produced from organic matter (Ref 10-13). Moreover, fibrous filters have low removal efficiency, reuse capacity and poor mechanical strength properties thus affecting filter performance and durability. Porous ceramic membrane filters have superior performance in hot flue gas filtration due to high removal efficiency, manipulation of pore size, high-temperature stability, and corrosion resistance (Ref 13, 14). Highly porous microstructures can be obtained using mullite ceramics through the anisotropic growth characteristics via cross-linking and interlocking of mullite rods (Ref 15). This self-induced porous structure in mullite can be controlled by the preparation method (Ref 15). Additionally, mullite offers low thermal expansion, shock resistance, corrosion resistance, and high-temperature mechanical stability which are crucial for filter operations (Ref 16). Mullite is the stable aluminosilicate phase in the SiO_2-Al_2O_3 binary system (Ref 17), typically produced from chemical powders, industrial waste, and aluminosilicate minerals such as kaolinite, kyanite, sillimanite, andalusite and pyrophyllite (Ref 18-20). Zhou et al. (Ref 21) prepared porous silica/mullite ceramics using silicon kerf waste as raw material, while Liu and Xiang (Ref 22) fabricated porous mullite by recycling photovoltaic waste. Chen et al. (Ref 23) investigated the mechanical properties of porous mullite ceramics prepared by selective laser sintering of mullite powder mixed with MnO_2 and phenolic resin. Hulse and Graf (Ref 24) showed that pyrophyllite decomposes into mullite and silica phases at temperatures over 1050 °C.

Pyrophyllite has high-temperature strength in a dehydrated state. Mukhopadhyay et al. (Ref 25) demonstrated that pyrophyllite contains low alumina and high silica resulting in the formation of mullite and amorphous silica when heated.

Nthabiseng Ntholeng, Patrick Rokebrand, and **Iakovos Sigalas**, Department of Chemical, Metallurgical and Materials Engineering, Tshwane University of Technology, Pretoria, South Africa; and **Nthape Percyval Mphasha**, Department of Chemical, Metallurgical and Materials Engineering, Tshwane University of Technology, Pretoria, South Africa; and School of Chemical and Metallurgical Engineering, University of the Witwatersrand, Johannesburg, South Africa. Contact e-mail: sthabi@gmail.com.

Mullite crystallization from pyrophyllite is also easier than from kaolinite. Rieger et al. (Ref 26) observed that high-sericitic pyrophyllite may form mullite at comparatively low temperatures, resulting in increased fired strength. Mullite with high hardness and fracture toughness were achieved at a temperature of 1600 °C and soaking time of 20 minutes when spark plasma sintering was used (Ref 27). Particle stacking (Ref 28), pore-forming agent addition (Ref 29), sacrificial templating (Ref 30), foam-gelcasting (Ref 31) and freezing casting (Ref 32) are some of the fabrication methods used to make porous ceramics. Reaction sintering is the preferred technique as it produces porous mullite ceramics directly from aluminosilicate minerals. Moreover, addition of high activity α-Al_2O_3 is key in the formation of secondary mullite and enhances porosity through consumption of the glassy phase (Ref 33). Although various fabrication methods have been reported in the literature, to the author's knowledge, no research has been conducted on the direct fabrication of porous mullite ceramics from mullite grains. The interlocked structure of mullite grains is not only inherently porous but favorable for high mechanical strength and high-temperature applications useful in hot–gas filtration.

This research investigates the fabrication of porous mullite filter material from reaction sintered mullite grains. Ammonium hydrogen carbonate and polyethylene glycol (PEG 400) were added to mullite grains as pore-former and binder, respectively. The impact of grain morphology on the structural integrity of a porous structure is studied, as well as the effect of sintering temperature on particle bonding and diffusion at the grain boundary. The mechanical properties of the porous mullite filter material were studied to determine their suitability for hot gas filtration.

2. Materials and Methods

2.1 Materials Preparation

2.1.1 Mullite Mix. Light gray pyrophyllite with average particle size of 3.5 μm, mined by Wonderstone in Ottosdal, South Africa, was dehydroxylated at 800 °C for 30 min with heating and cooling rate of 5 °C/min. Submicron α-Al_2O_3 (P172SB) of 99.7% purity (CER Advance Engineering Ceramics (Pty) Ltd, South Africa) and calcined pyrophyllite were mixed with iso-propanol in an attrition mill 01-HD model (Union Process, USA) for 2 h using 4.5-mm alumina balls (Anton Paar GmbH, Germany). The ball-to-mass ratio was 1:5. The mix was calculated on the stoichiometric basis to provide the molar ratio of 3:2 mullite ($3Al_2O_3$:$2SiO_2$). The slurry was dried in a rotary evaporator at 150 rpm for 30 min. Milled powder was compacted in a stainless-steel die using an HP-3560-20 uniaxial hot press (Thermal Technology Inc, USA) at 100 MPa for 5 min to form green body compacts. The compacted pellets were 20 mm in diameter and 5 mm thick. The green compacts were then sintered in a LHT 04/18 muffle furnace (Nabertherm GmbH, Germany) at 1600 °C, the applied heating rate was 5 °C/min, and holding time was 1 and 3 h. Powder x-ray diffraction (XRD) was used to characterize the crystal structure of the sintered samples.

2.1.2 Mullite Mix Granulation. Granulation of mullite mix powder was done to control porosity and surface-to-volume ratio as the sintered mixed mullite powder did not show a porous structure. Mullite mix (light gray pyrophyllite and α-Al_2O_3) was granulated in a beaker with 1 wt.% polyethylene glycol (PEG) 400 by slowly adding water while continually stirring. The granules formed were initially sieved between 150 and 300 μm but shrinkage during sintering meant sieving between 300 and 500 μm gave a better mullite particle size. Mullite mix granules were mixed with ammonium hydrogen carbonate (40 vol.%) (Sigma-Aldrich SA (PTY) LTD) in a T2F turbula mixer (Glen Mills, USA) for 2 h to ensure homogeneity. The granulated mullite mix was compacted in a steel die using an HP-3560-20 uniaxial hot press at pressure 1, 5, and 10 MPa for 30 min to form green compacts and sintered at 1600 °C for 3 h. It was observed that the sintered compacts formed from mullite mix powder resulted in friable clogged filter material. To avoid the formation of a friable clogged filter material due to mullite mix granules being crushed during compaction, mullite mix granules sieved to 300-500 μm were pre-reacted at 1600 °C for 3 h to give hard semi-mullitized granules with improved structural integrity for handling. Samples were then pressed using 1 wt.% PEG400 at 1, 5, and 10 MPa before being sintered at 1600 °C for 3 h.

2.1.3 Mullite Filter. Pre-reacted mullite (with 3 wt.% PEG 400) and mullite mix granules were mixed with ammonium hydrogen carbonate (40 vol.%), pressed at 20 and 30 MPa for 30 min and sintered at temperatures from 1700 to 1800 °C in the muffle furnace. To avoid crushing, the pre-reacted grains tap compaction was performed by placing the grains in a die while tapping the sides to ensure close packing which proved to be unsuccessful. Schematic diagram of the fabrication process is shown in Fig. 1.

2.2 Characterization of the Sintered Samples

Phase compositions were identified by x-ray diffraction (Bruker D2 Advance diffractometer, USA) with copper as the anode material at 30 kV and 10 mA. The samples were scanned at a step scan mode of 0.02°. Diffractograms were collected over a 2θ range between 10° and 90° at room temperature. PANalytical model AXIOS x-ray fluorescence spectrometer at 50 kV and 50 mA (Malvern Panalytical, UK) was used to characterize the chemical composition of as-received pyrophyllite powder. The analysis was performed by superQ software. The microstructure and morphology of porous filter material coated with a combination of carbon and gold-palladium was examined with Carl Zeiss Sigma Field Emission Scanning Electron Microscope (FESEM) equipped with Oxford x-act EDX detector (Carl Zeiss Microscopy GmbH, Germany). Light microscopy (Nikon SMZ745T, Netherlands) was used to collect images of the sintered materials. Density measurements of the sintered samples were calculated from sample weight and dimensions. Compressive strength was measured at room temperature using an Instron 1175 Tensile/Compression test machine (Instron, USA). The pore size distribution of samples was examined by Mercury Porosimetry (MicroActive AutoPore V, Micromeritics, USA).

3. Results

3.1 Phase Analysis

The as-received pyrophyllite powder (Fig. 2a) has flaky irregular particles with agglomerates, whereas the α-Al_2O_3

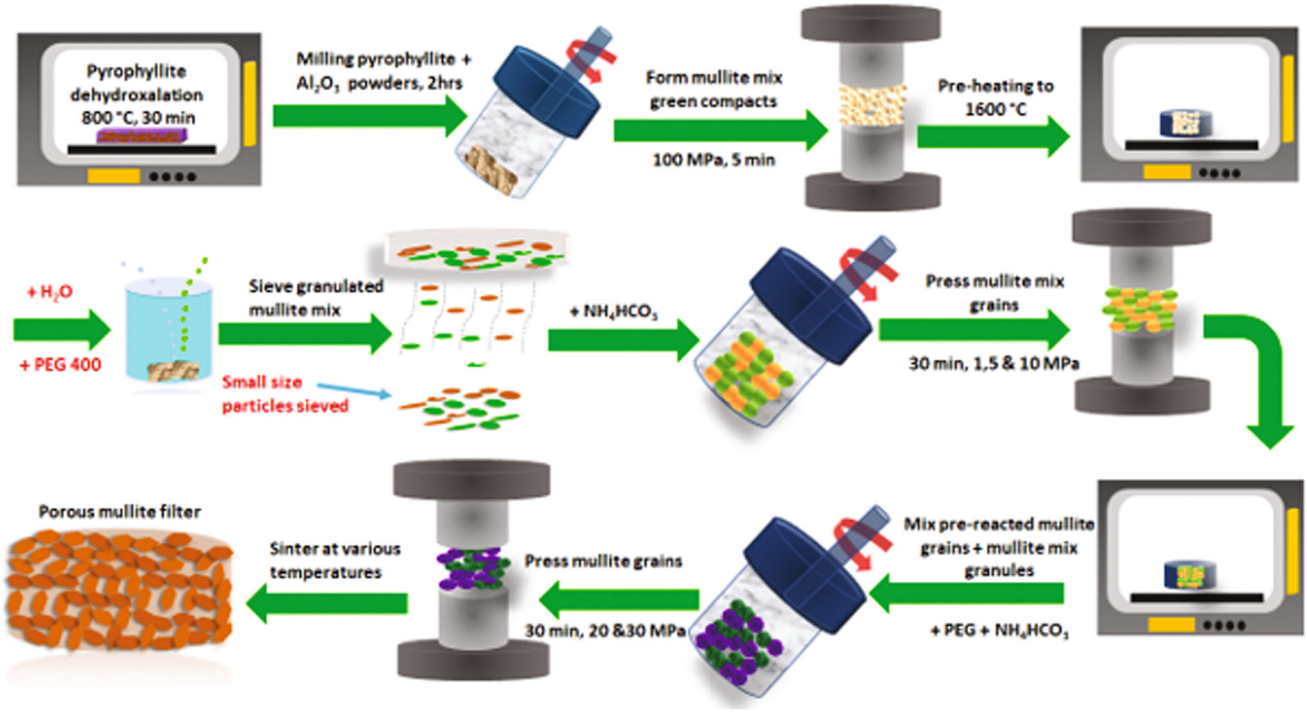

Fig. 1 Schematic diagram illustrating the fabrication process for porous mullite ceramic filter

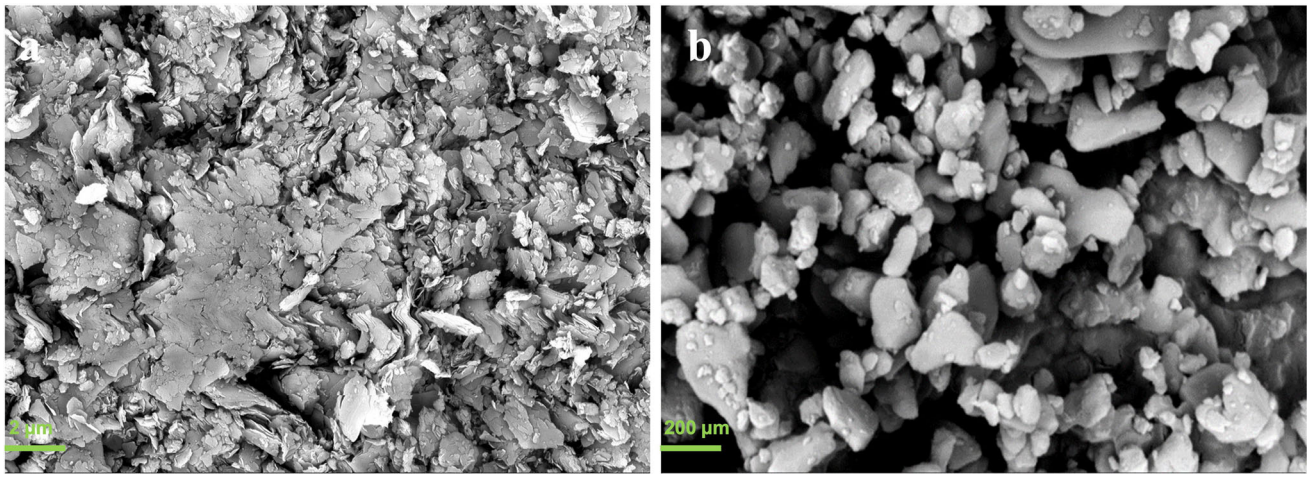

Fig. 2 SEM of the (a) as-received pyrophyllite powder and (b) as-received Al_2O_3

powder (Fig. 2b) has irregularly shaped particles of varying sizes. The main phase is pyrophyllite, with minor phases of quartz and stishovite (Fig. 3). The diffraction pattern (Fig. 3) of the as-received α-Al_2O_3 shows no impurities indicating pure Al_2O_3 phase. The chemical composition (Table 1) of as-received pyrophyllite powder constituted mainly by silica and alumina, with trace amounts of K, Ti, Fe, Mn, Mg, Ca, Na, Cr and P oxides.

A stoichiometric mixture of pyrophyllite and Al_2O_3 was sintered at 1600 °C at various sintering times. Powder x-ray diffraction was used to investigate the crystal structure of the sintered material. The resultant diffraction pattern (Fig. 4) shows short (1 h) and long (3 h) sintering times. At low sintering time (1 h), thermal decomposition of pyrophyllite to mullite is not observed. Instead, a mixture of andalusite, aluminum oxide, iron silicate, and stishovite phases is observed, with andalusite dominating. Increasing the sintering time to 3 h resulted in complete mullitization. This shows that longer sintering times at 1600 °C are required to obtain a pure mullite phase.

Upon determining the sintering parameters, a mixture of granulated mullite mix, binder (PEG 400), and pore-forming agent (ammonium bicarbonate) was sintered for 3 h at 1600 °C for samples compacted at (a) 1 MPa, (b) 5 MPa, and (c) 10 MPa. The granulated mixture had particle sizes ranging from 300 to 500 μm. The sintered samples were imaged using optical light microscopy (Fig. 5). All sintered samples had fine, loosely bound particles on the surface, which is detrimental for filter material because it could cause clogging. A lower compaction pressure (1 MPa) resulted in a better filter material

but poor particle bonding. Increasing compaction pressure produced samples with better structural integrity, with 10 MPa being the best. The resulting smearing from the die contact suggests that granules are crushed during compaction causing little or no porosity. This also suggests that the mullite mix grains have poor structural integrity.

3.2 Effect of Grain Morphology

Microstructure analysis of the semi-mullitized grains and the mullite mix grains (Fig. 6) indicated that the heat-treated grains were firm and could not be hand-crushed. In contrast, the untreated grains could be easily crushed. Pre-heated grains (Fig. 6a) are larger and more defined than unheated grains (Fig. 6d), which have a mixture of fine and irregular large grains. Zooming in on a single pre-heated grain reveals a porous interlocked structure made up of a mixture of small spherical, short columnar, and acicular grains (Fig. 6c).

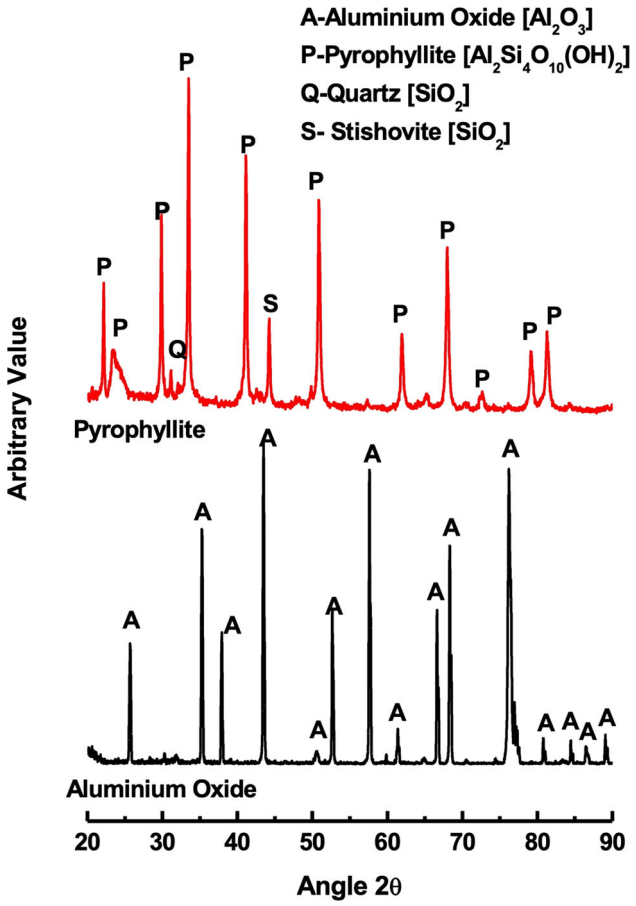

Fig. 3 XRD analysis of the as-received pyrophyllite powder and as-received Al_2O_3 Powder

Untreated grains show a mixture of spherical, flaky, and irregular-shaped grains at high magnification (Fig. 6f). According to the results, heat treatment promotes grain growth and morphological evolution. Morphological evolution is characteristic of microstructural mullite.

Pre-treating mullite mix grains produced hard granules that can be washed with iso-propanol to remove fine dust from the surface. This is particularly important in hot gas filtration where small particulates tend to clog the pores and cause poor filter performance. Further, the formation of interlocked rod-like grains with a high aspect ratio and strength enables for the creation of a porous structure with good mechanical properties.

Pre-heated grains were mixed with mullite mix powder. Upon being pressed with 1 wt.% PEG400 at 20 MPa, samples were then sintered at 1600 °C for 3 h. The microstructure of the sintered mullite filter is shown in FESEM micrographs (Fig. 7), which includes a porous compact structure and an interlocked network structure made up of a mixture of columnar, spherical, and rod-like grains.

Small grains are poorly bound at the surface of large grains, whereas large grains are strongly bonded and have good contact at grain boundaries. Poorly bonded particles have poor mechanical properties and may act as crack initiators. Furthermore, the sintering temperature of 1600 °C was insufficient to achieve high diffusion at the point of contact between the grains. Higher sintering temperatures are required to enhance the diffusion at the contact points.

After obtaining an interconnected network of rod-like mullite grains, tap compaction was performed. The tap compacted grains were sintered for 3 h at 1700 °C without being mixed with a pore-forming agent (ammonium hydrogen carbonate). This was ineffective due to the combination of bulk sample shrinkage and, more importantly, individual granule shrinkage, which caused most of them to pull apart. As a result, it was determined that proper compaction was required. Even though small grains were formed; they aided in the removal of the excess loose powder at the surface.

3.3 Effect of Sintering Temperature

High compaction pressure and additional binder were required due to the firmness of the pre-reacted grains to obtain compacts with good structural integrity. The PEG content was increased from 1 to 3 wt.%, and the compaction pressure was raised from 20 to 30 MPa. Thereafter, a filter material was compacted at 30 MPa and sintered for 3 h at 1700 °C. Microstructural analysis of the sintered compacts at 1700 °C (Fig. 8) was conducted. Increasing the compaction pressure to 30 MPa did not break the granules and yielded a stable compact. Sintering temperature of 1700 °C resulted in friable samples. Large tunnel-like pores in the microstructure (Fig. 8) suggested that mechanical properties may be poor. Additionally, these tunnel-like pores separated the large agglomerates consisting of small and large grains.

Table 1 Chemical composition, wt.% of the as-received pyrophyllite powder

Mineral	SiO_2	Al_2O_3	Fe_2O_3	FeO	MnO	MgO	CaO	Na_2O	K_2O	TiO_2	P_2O_5	Cr_2O_3	LOI
Wt.%	58.63	30.30	0.12	0.99	0.01	0.07	0.05	0.17	1.09	1.94	0.15	0.03	6.06

LOI = Loss in ignition

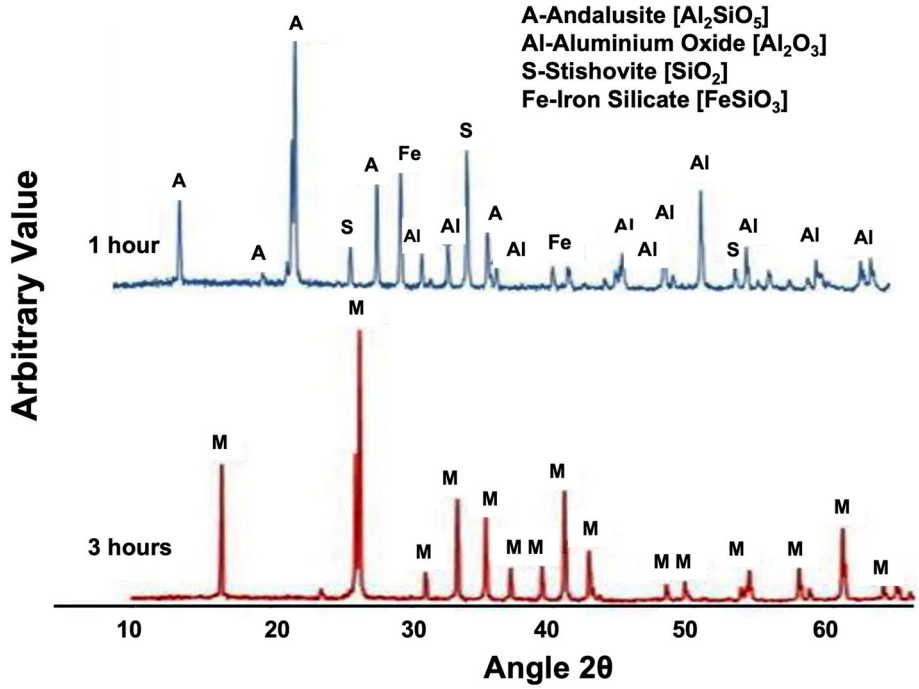

Fig. 4 XRD pattern of mullite mix sintered at 1600 °C for 1 h (top) and 3 h (bottom).

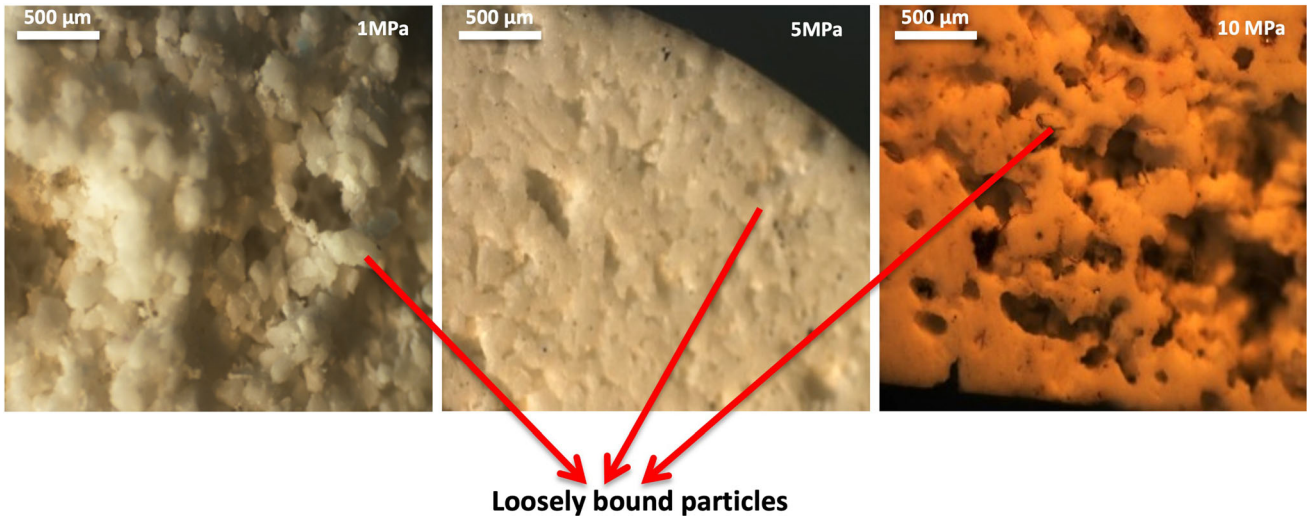

Fig. 5 Optical microscopy images of ammonium bicarbonate + mullite mix + binder pressed at (a) 1 MPa (b) 5 MPa (c) 10 MPa sintered for 3 h at 1600 °C.

The sintering temperature was further increased to 1750 and 1800 °C, resulting in a porous interconnected network structure. The effect of sintering temperature on grain growth was determined by measuring the average diameter and length of at least 100 grains on SEM images. The average particle diameter increased from 2.63 to 3.49 μm (Fig. 9) when the sintering temperature was raised from 1750 to 1800 °C. The length of rod-like mullite grains grew from 7.11 to 11.67 μm (Fig. 9). Figure 10 shows that particle bonding at the boundaries was enhanced as the amount of the glassy phase increased. Besides, crystals have lots of growth steps and stacking faults on their tips.

3.4 Mechanical Properties

According to the mercury intrusion porosity (MIP) analysis, the filter material sintered at 1800 °C showed better structural integrity. This was confirmed by studying the bimodal pore size distribution and the low pore size range (Fig. 11). The largest narrow peak shows a pore size of 29.32 μm, whereas the second peak has a pore size of 1.15 μm. The peak in the low pore size range suggested that structural hysteresis in that pore range caused a delayed retraction as mercury snap-off during the initial stages of pressure reduction [14]. Furthermore, the filter's narrow pore size distribution suggested that the filter

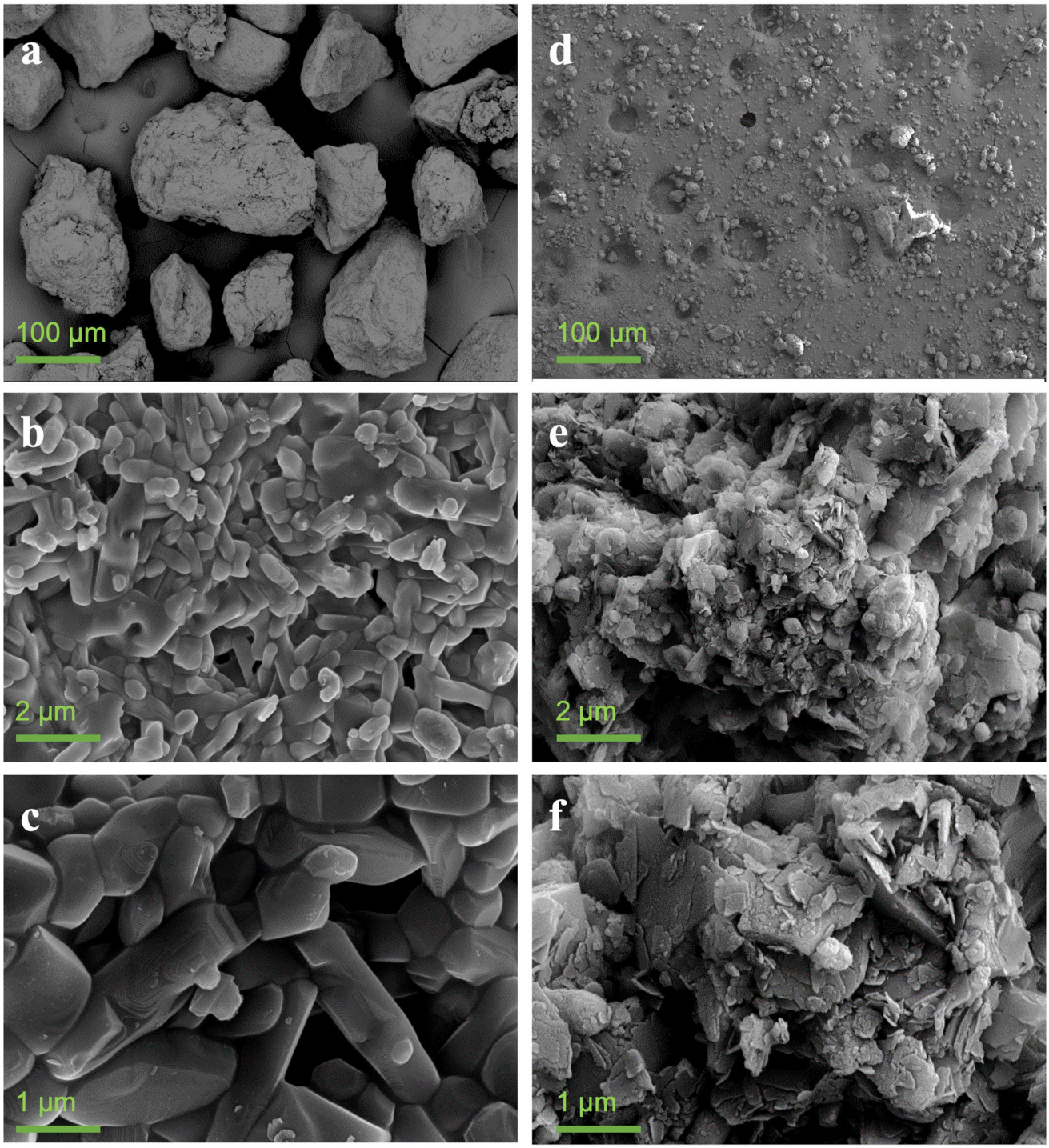

Fig. 6 FESEM micrographs of (a-c) pre-reacted mullite mix grains at 1600 °C and (d–f) unheated mullite mix grains.

could be used for the microfiltration of gases containing fine particles. At 1800 °C, the filter material had an overall porosity of 36.20% and an average pore diameter of about 29.32 μm. The bulk density of the sintered filter material was 1.99 g/cm^3, corresponding to a relative density of 65.25%. Low density was expected as the material is highly porous.

Compressive strength tests were carried out to better understand the material's mechanical properties. Materials representative of 31 samples were compressed along the height direction at room temperature according to ASTM C1424-15 (Ref 34). Table 2 shows that the minimum compressive strength and maximum compressive strength measured are 5.97 and 20.71 MPa, respectively.

The fluctuations in the compressive stress versus compressive extensions curves were caused by micro-cracking during the compression tests, as shown in Fig. 12. For all the tests, the average strength for all tests was found to be 12.75 MPa, indicating that the fabricated materials have good structural integrity. In addition, an estimation of the Weibull distribution of strength was estimated. The Weibull plot indicates a straight

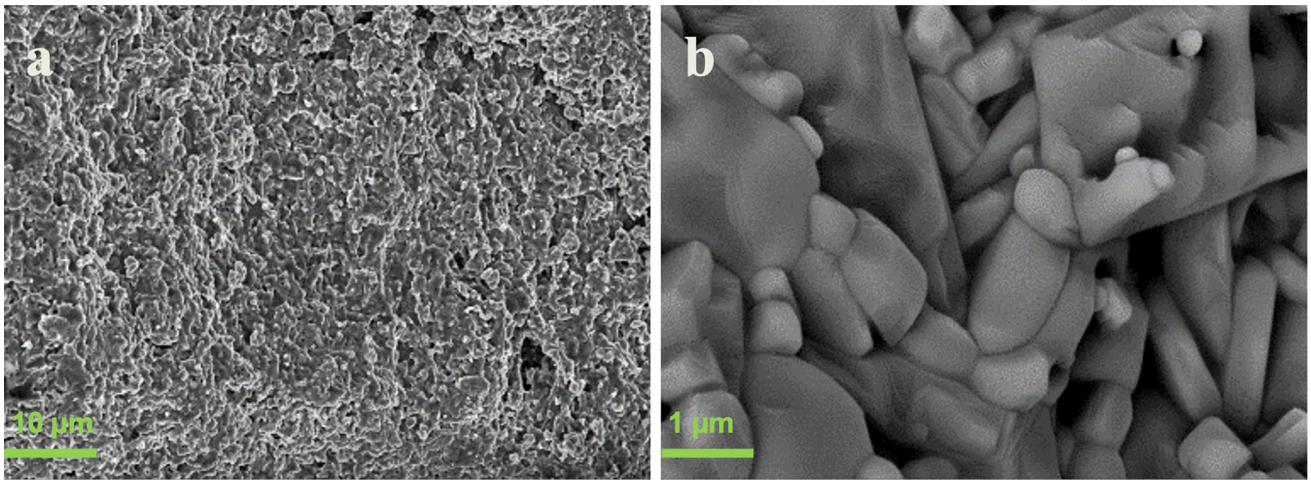

Fig. 7 FESEM micrographs of mullite filter pressed at 20 MPa sintered at 1600 °C for 3 h. (a) Low magnification. (b) High magnification.

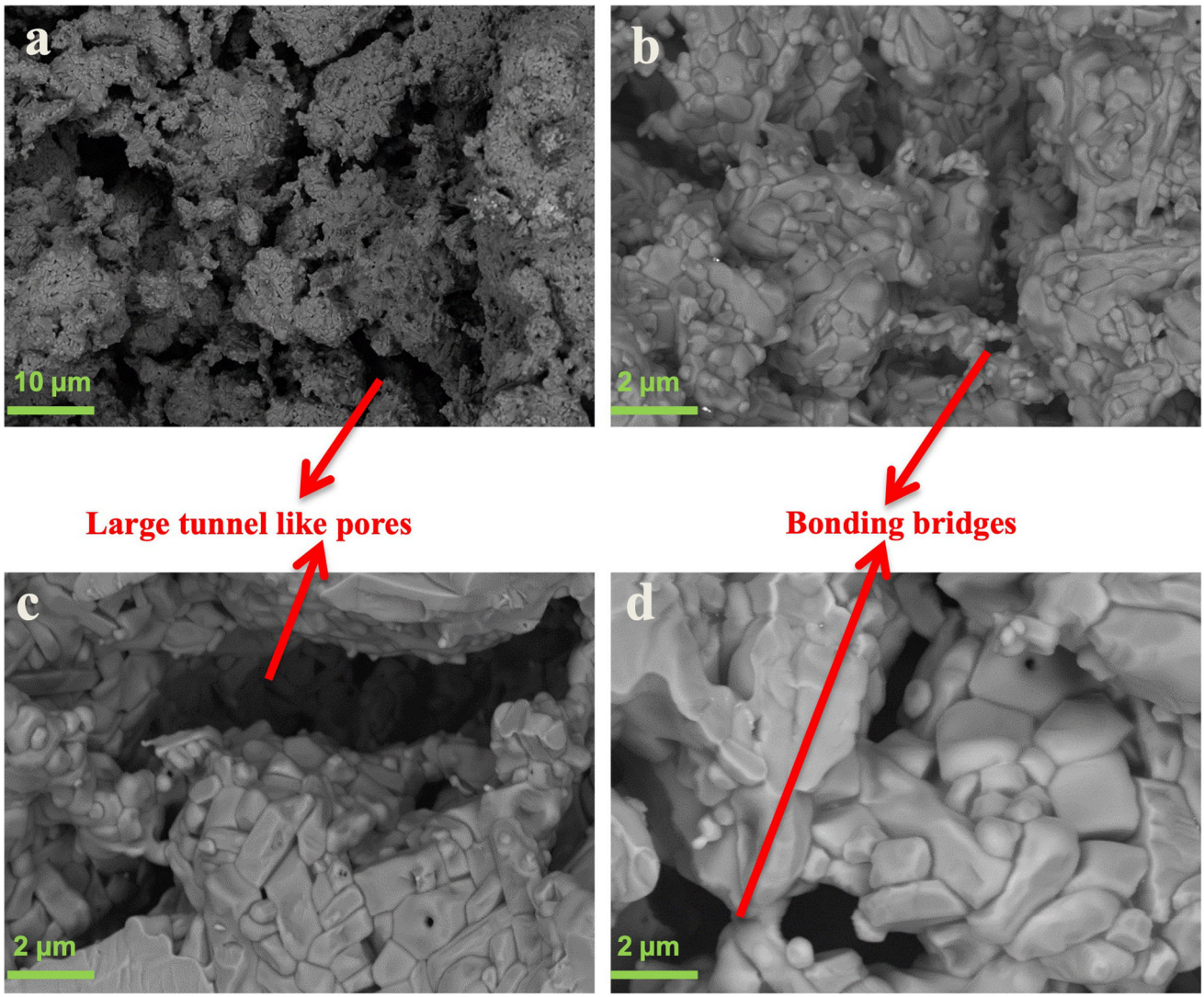

Fig. 8 FESEM micrographs of mullite filter pressed at 30 MPa sintered at 1700 °C for 3 h (a–d).

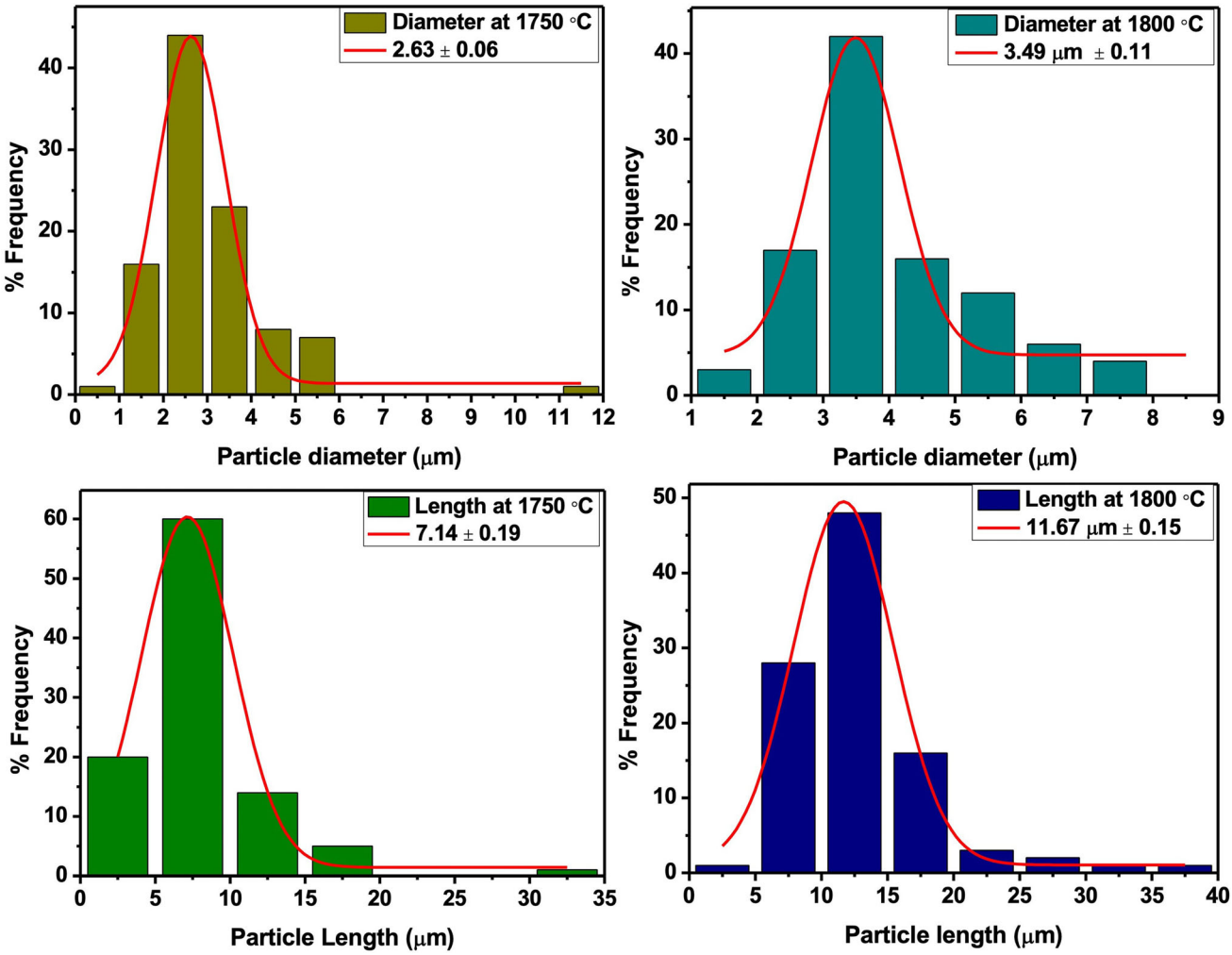

Fig. 9 Average particle diameter and length measured from SEM microstructure of the filter material sintered at 1750 and 1800 °C for 3 h.

line with a positive slope and a Weibull modulus of 2.67 (Fig. 13). The characteristic strength was measured to be 14.49 MPa.

4. Discussion

Sintering temperature of mullite was determined according to the phase diagram of SiO_2-Al_2O_3. Based on the SiO_2-Al_2O_3 phase diagram shown in Fig. 14, formation of pure mullite phase is dependent on the Al_2O_3 and SiO_2 composition and the sintering temperature. In this study, sintering temperature of 1600 °C was used as the intention was to fabricate pure mullite phase. Since pyrophyllite contains high SiO_2 content, an additional Al_2O_3 was added to achieve 3:2 ($3Al_2O_3.2SiO_2$) stoichiometry mullite which allows for the formation of pure mullite phase at temperature of 1600 °C.

The formation of mullite phase from a mixture of pyrophyllite and Al_2O_3 (Fig. 4) is dependent on sintering time. With a shorter sintering time, andalusite is the most prevalent phase with the formation of impurities. Furthermore, formation of the andalusite phase shows that there is a gradual diffusion of Al ions into SiO_2 glassy phase taking place, while mullite nucleation seems to be sluggish which could be due to the bond strength of α-Al_2O_3 dictating the dissociation of Al_2O_3 molecules (Ref 36). This is consistent with Pereira's (Ref 37) findings who observed that α-Al_2O_3 in the presence of amorphous SiO_2 is inert up to 1400 °C. The formation of Fe_2SiO_2 could be attributed to the presence of Fe_2O in pyrophyllite. The stoichiometric mixture of pyrophyllite-alumina produced a pure mullite phase at 1600 °C which seems to occur at higher temperature compared to the kaolinite-alumina system, where primary mullitization is achieved around 1300 °C (Ref 38). By increasing the sintering time to 3 h, a pure mullite phase was formed, indicating secondary mullitization. Secondary mullitization was characterized by an increase in both dissolubility and the saturation point of aluminum, which increased the liquid with aluminum ions (Ref 39). These findings are in agreement with Triphathi et al. (Ref 40) who reported that there is mullite conversion after 1.5 h at 1600 °C.

Upon establishing the sintering parameters, a mullite filter was manufactured by forming compacts with mullite pre-reacted grains. The compaction pressure had an adverse effect on the grains, resulting in production of a clogged filter material that is structurally poor. This indicated that the produced mullite mix grains had low strength in all sintered material. Coble and Kingery (Ref 41) studied the microstructure and mechanical properties of porous aluminas-based materials with

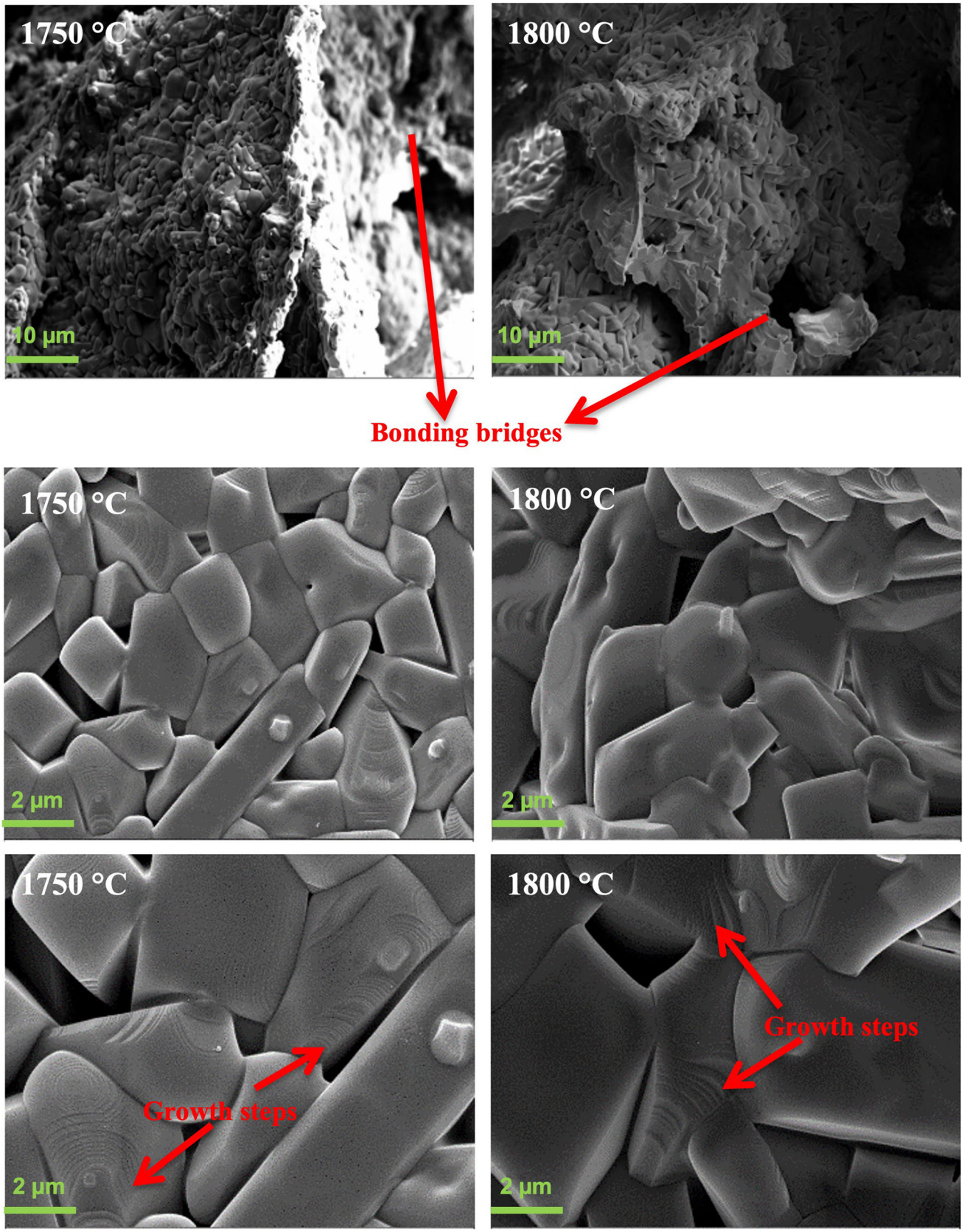

Fig. 10 FESEM micrographs of mullite filter pressed at 30 MPa sintered at 1750 and 1800 °C for 3 h.

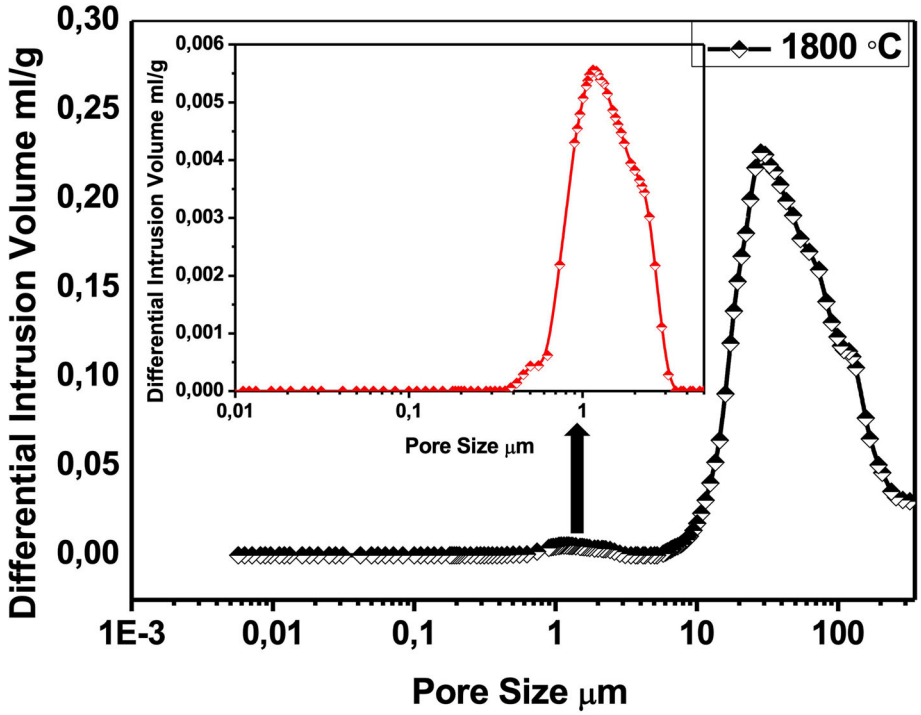

Fig. 11 Differential intrusion vs pore size plot of the filter material sintered at 1800 °C.

Table 2 Measured compressive strength and maximum compressive extension

Number of specimens: 31	Maximum compressive extension, mm	Compressive strength, MPa
Minimum	0.70	5.97
Maximum	1.38	20.71
Average	1.07 ± 0.20	12.63 ± 2.98

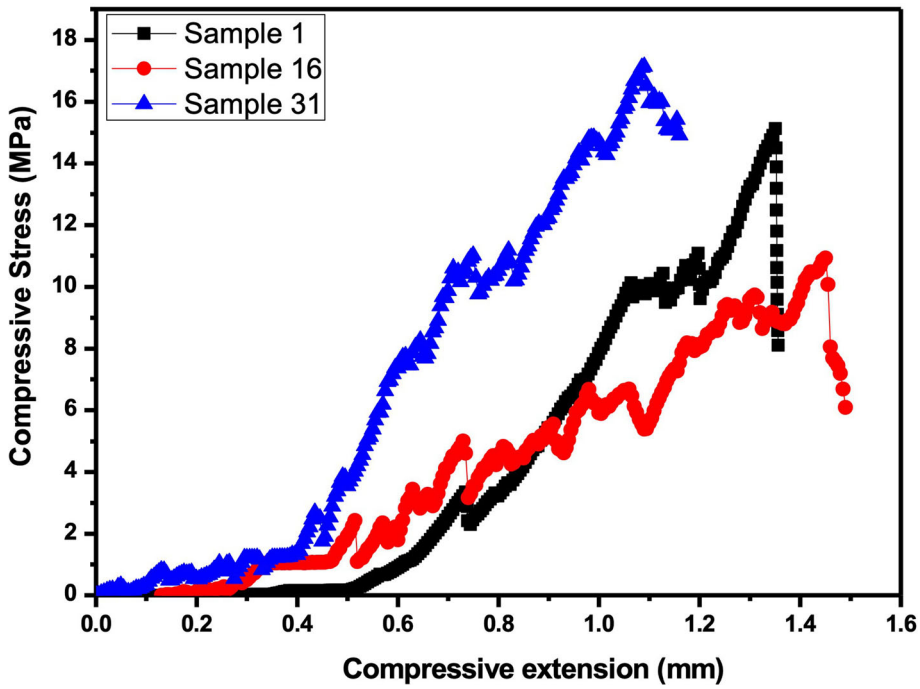

Fig. 12 Compressive strength vs compression extension of filter material sintered at 1800 °C.

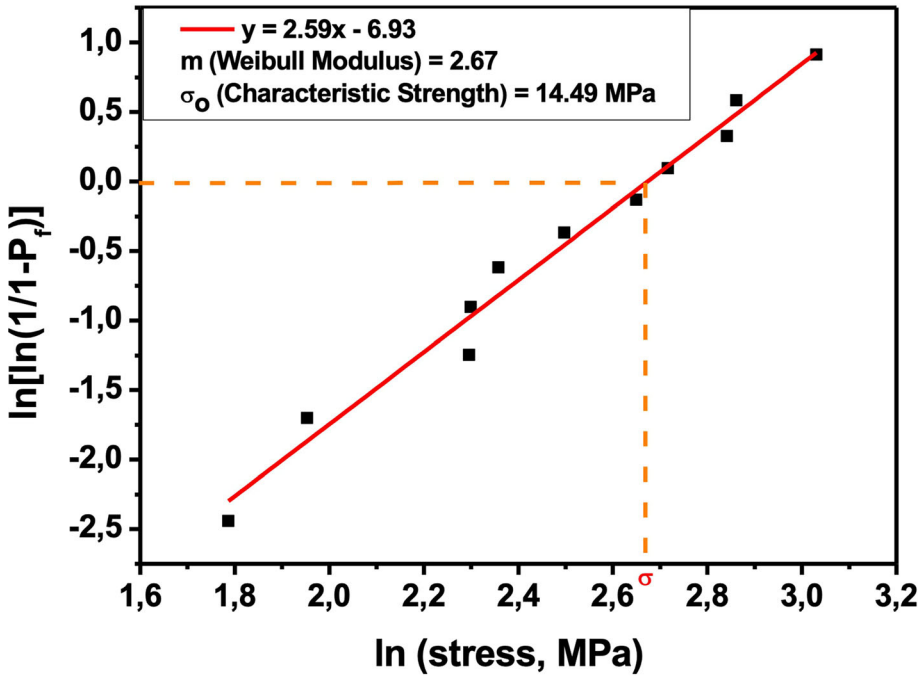

Fig. 13 Weibull modulus plot for filter material sintered at 1800 °C.

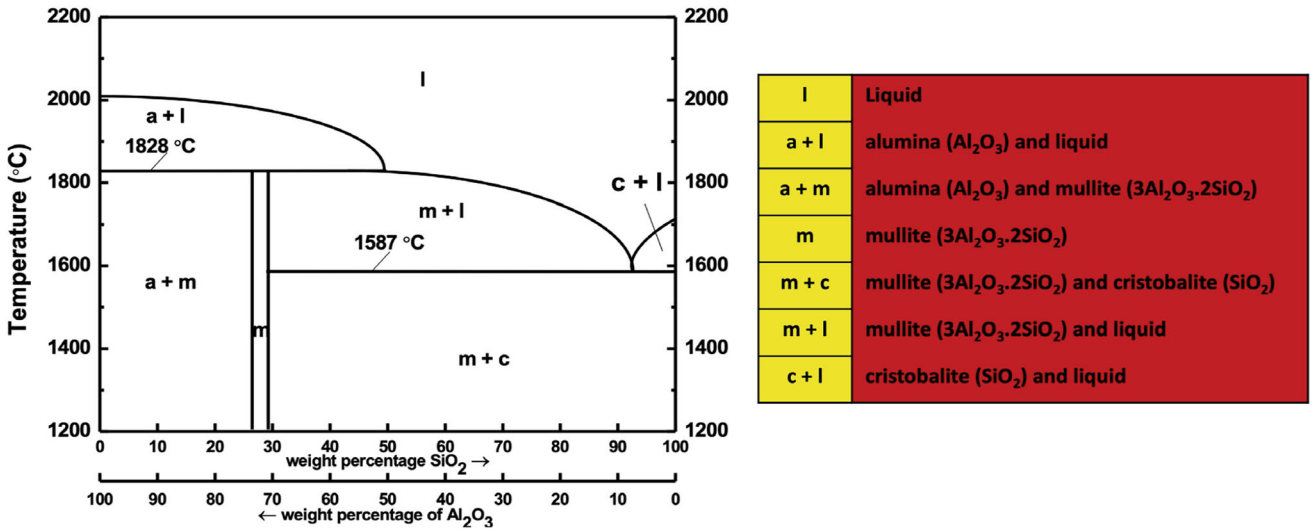

Fig. 14 Phase diagram of Al_2O_3-SiO_2 system adapted from (Ref 35).

traditional, isotropic porous microstructures. The elongated acicular mullite (ACM) crystals showed a low percolation threshold, which is described as a volume fraction at which the solid phase becomes interconnected. The results revealed that, at a given porosity, a more interconnected microstructure may be observed for materials with low percolation threshold compared to the spherical counterpart. Moreover, finite element and homogenization techniques have proven that increased connectivity resulted in increased stiffness at a given porosity (Ref 42). By changing the grain morphology, the mullite mix grains were heat-treated to enhance grain stiffness. Heat-treating the mullite mix grains to 1600 °C yielded a mixture of porous interlocked structure consisting of a mixture of small spherical, short columnar, and rod-like mullite grains. The observed morphology progression is characteristic of microstructural mullite (Ref 38, 43). The identified microstructural mullite consists of either equiaxial grains or elongated grains (Ref 44). In general, the mullite grains are platelike, columnar, or acicular in shape. According to the work of Aramaki and Roy (Ref 45) and Aksaf and Pask (Ref 46), the Al_2O_3-SiO_2 phase diagram indicates that the formation of a liquid phase occurs above eutectic temperature (1590 ± 10 °C) and when silica-rich composition in the two-phase field is used. At high temperatures, silica converts to silicate liquid and to a glassy phase during cooling. The formation of elongated mullite grains at 1600 °C in present study agrees with the literature.

To achieve structurally sound filter material, pre-reacted grains required a higher sintering temperature and higher compaction pressure to allow diffusion at the grain boundaries.

A higher sintering temperature (1700 °C) was attempted, and the resulting filter material was friable with a large tunnel-like pore visible (Fig. 8). This may be attributed to a combination of pores produced by pore-former agent, the reduction in aspect ratio and the quantity of rod-like mullite grains (Ref 47). The lower amount of acicular grains reduces their effects of filling and splitting pores, resulting in increased pore size (Ref 47). Moreover, the interaction of Al_2O_3 and SiO_2 caused a reduced aspect ratio of mullite grains. In comparison with γ-Al_2O_3, ρ-Al_2O_3, and $Al(OH)_3$, the driving force for grain growth in a stable material such as α-Al_2O_3 is comparatively low. As the driving force decreases, the amount of mullite grains gradually decreases (Ref 48). Furthermore, Huang et al. (Ref 44) demonstrated that elongated mullite grains are formed after 1 hour and longer heat treatments yields abnormal grain growth resulting into formation of blocky grains. Large rod-like and tubular grains are well bonded at grain boundaries by a glassy phase in comparison with the small grains which are adsorbed on the surface. Michel et al. (Ref 49) prepared mullite whiskers by directional solidification and described growth direction as c-axis while they were bounded by {110} or {111} planes, respectively. Furthermore, anisotropic growth of elongated grains takes place in the {001} direction for a minimization of the free energy (Ref 50). The growth mechanism is linked to the crystal structure of mullite which comprises AlO_6 chains aligned in the c-direction and cross-linked by AlO_4 and SiO_4 tetrahedra at the corners (Ref 50).

Increasing the sintering temperature from 1750 to 1800 °C resulted in grain growth, with an average diameter increasing from 2.63 to 3.49 μm and length increasing from 7.11 to 11.67 μm (Fig. 9). As the grain size increased, there was also an increase in the formation of a glassy phase at grain boundaries, which appeared to have enhanced particle bonding. The excess silicate liquid visible in the micrograph (Fig. 10) can be attributed to the exceptional stability of α-$A1_2O_3$, which reacts poorly with SiO_2 (Ref 38). Furthermore, the crystals show lots of growth steps and stacking faults on their tips (Fig. 10). The formation of stacking faults is characterized by the two-dimensional nucleation mechanism of mullite crystals as observed by Goski and Caley (Ref 48). Two-dimensional nucleation mechanism typically occurs when the critical size nuclei first forms on a flat crystal surface, followed by the simultaneous growth and the formation of further critical nuclei (Ref 41). The size and contact angle of adsorbed particles have a direct impact on the free energy barrier which affects the nucleation rate and growth kinetics (Ref 41). After the formation of secondary mullite, two-dimensional heterogeneous nucleation takes place in acicular mullite crystals. Secondary mullite is formed when a glassy phase of SiO_2 reacts with α-Al_2O_3 (Ref 47). The generated incipient crystals of secondary mullite then nucleate at the growth steps or flaws of primary mullite surfaces by heterogeneous nucleation (Ref 38). Therefore, it can be assumed that mullite occurs in two-dimensional nucleation mechanism in the present study since the growth steps and stacking faults are seen in the mullite grains. Although primary mullitization was not detected by XRD in the present study, Pereira et al. (Ref 37) showed that primary mullitization from the reaction of SiO_2 with α-Al_2O_3 occurs after 1.5 h. Therefore, it is assumed that primary mullitization may have occurred after 1 h prior to observing the secondary mullitization after 3 h. The growth occurred by layers along primary mullite surfaces until the entire steps were completely covered, resulting in coarsening of the primary mullite surface. This indicated that the roughening temperature was reached when the sintering temperature was increased to 1800 °C.

Mechanical properties of filter material sintered at 1800 °C were evaluated. The average compressive strength was 12.75 MPa, with an overall porosity of 36.20%. Zhou et al. (Ref 21) reported compressive strength of 3.19-8.14 MPa for porous silica/mullite ceramics which is lower than the obtained value in present study. Recently, Dong et al. (Ref 51) reported permeation of 4.82×107 L m^{-2} h^{-1} bar^{-1} for mullite-bonded SiC filter with compressive strength of 12.1 ± 0.5 MPa and 64.8% porosity. By increasing the porosity level to 80.5%, compressive strength dropped to 4.2 ± 0.1 MPa, while permeation increased to 7.44×107 L m^{-2} h^{-1} bar^{-1}. This indicates that mullite grains can be used in fabrication of structurally sound porous mullite ceramics though optimization may be required to enhance porosity while maintaining strength. The low compressive strength in the present case can be attributed to poor structural integrity, which resulted from poor particle packing efficiency during compaction. Compaction of granules is affected by particle size and shape in the pressing powder (Ref 52). Furthermore, it is influenced by particle packing parameters, the friction, and lubrication of the particle surfaces, which control the stiffness of the granules (Ref 52). While this was not observed in the current study, the binder may have acted as a lubricant and decreased the chances of particle deformability. Tartak et al. (Ref 53) studied the effect of PEG binder on microstructural and mechanical properties. The results showed that the strength increased rapidly until a certain point before beginning to decline when 3 wt.% PEG was used. It was also established that large grains and large pores lead to a rapid loss of strength (Ref 53). This means that, as observed in the current study, the granules with a high binder concentration were resistant to deformation during compaction. This is despite the tendency of porous mullite ceramics manufactured from raw powder material exhibiting a brittle fracture mechanism (Ref 54). Although pore-former was added, the fabrication method used to manufacture the porous materials also allows for control over porosity. While the effect of pore-former was not studied, it is suspected if it is undertaken may give light into how to control porosity.

Weibull modulus, also known as shape parameter of the strength distribution, is a measure of the material's strength diversity (Ref 55). The obtained Weibull modulus value of 2.67 indicates large scatter in strength (Ref 56). This suggests that the produced filter material exhibited low structural reliability. However, the measured characteristic strength of 14.49 MPa suggests that the filter material has potential through the optimization of manufacturing conditions.

5. Conclusions

Reaction sintering of pyrophyllite clay and α-Al_2O_3 at 1600 °C for more than 1 h produced a single mullite phase as determined from XRD. Heat-treating granulated mullite mix at 1600 °C resulted in a change in grain morphology which improved the structural integrity of the porous mullite filter. Improved grain strength required an increase in binder content, compaction pressure, and sintering temperature. Sintering temperatures above 1700 °C induced growth of rod and blocky

mullite crystals via 2-D heterogeneous nucleation. At temperatures just below 1800 °C, the produced porous structure was friable and had poor structural integrity. At 1800 °C, enhanced structural integrity of porous material was achieved with measured density of 1.99 g/cm^3 and relative density of 65.25%. The porous material with an overall porosity of 36.20% and average compressive strength of 12.75 MPa showed potential for application in hot gas filtration. However, the preliminary sintering results indicate that the methodology adopted in this study is energy intensive; hence, further investigations need to be done to reduce high sintering temperature and improve the mechanical properties.

Acknowledgments

The authors would like to thank the University of the Witwatersrand; the Microscopy and Microanalysis Unit (MMU) for XRD; Mr Nelwalani for SEM analysis and DST-NRF Centre of Excellence (CoE) in Strong Materials for funding.

Conflict of interest

The authors declare that they have no known competing financial interests or personal relationships that could have appeared to influence the work reported in this paper.

References

1. A. Pyzik, R. Ziebarth, C. Han, and K. Yang, High-Porosity Acicular Mullite Ceramics for Multifunctional Diesel Particulate Filters, *Int. J. Appl. Ceram. Technol.*, 2011, **8**(5), p 1059–1066
2. F. Zuo, S. Zhang, H. Liu, H. Fong, X. Yin, J. Yu, and B. Ding, Free-standing Polyurethane Nanofiber/Nets Air Filters for Effective PM Capture, *Small.*, 2017, **13**(46), p 1702139
3. R. Xiong, G. Sun, K. Si, Q. Liu, and K. Liu, Pressure Drop Prediction of Ceramic Membrane Filters at High Temperature, *Powder Technol.*, 2020, **364**, p 647–653
4. K. He and L. Wang, A Review of Energy Use and Energy-Efficient Technologies for the Iron and Steel Industry, *Renew. Sustain. Energy Rev.*, 2017, **70**, p 1022–1039
5. H. Wang, S. Lin, S. Yang, X. Yang, J. Song, D. Wang, H. Wang, Z. Liu, B. Li, and M. Fang, High-temperature Particulate Matter Filtration with Resilient Yttria-stabilized ZrO_2 Nanofiber Sponge, *Small*, 2018, **14**(19), p 1800258
6. R. Zhang, C. Liu, P.-C. Hsu, C. Zhang, N. Liu, J. Zhang, H.R. Lee, Y. Lu, Y. Qiu, and S. Chu, Nanofiber Air Filters with High-Temperature Stability for Efficient PM2.5 Removal from the Pollution Sources, *Nano Lett.*, 2016, **16**(6), p 3642–3649
7. S. Heidenreich, Hot Gas Filtration–A Review, *Fuel*, 2013, **104**, p 83–94. https://doi.org/10.1016/j.fuel.2012.07.059
8. A.R. Barron, "H. Schneider, K. Okada, and J. Pask. Mullite and Mullite Ceramics Wiley, Chichester, 1994, ISBN 0-471-94249-9. In: *Advanced Materials for Optics and Electronics*, Wiley 1995. pp 251
9. B.A. Latella, L. Henkel, and E.G. Mehrtens, Permeability and High Temperature Strength of Porous Mullite-Alumina Ceramics for Hot Gas Filtration, *J. Mater. Sci.*, 2006, **41**(2), p 423–430
10. E.H. Tanabe, P.M. Barros, K.B. Rodrigues, and M.L. Aguiar, Experimental Investigation of Deposition and Removal of Particles during Gas Filtration with Various Fabric Filters, *Sep. Purif. Technol.*, 2011, **80**(2), p 187–195
11. K.-S. Lee, J.-R. Sohn, and Y.-O. Park, Filtration Performance Characteristics of Ceramic Candle Filter Based on Inlet Structure of High-Temperature and High-Pressure Dust Collectors, *J. Ind. Eng. Chem.*, 2015, **21**, p 101–110
12. Y.-S. Chen, C.-J. Hsu, S.-S. Hsiau, and S.-M. Ma, Clean Coal Technology for Removal Dust Using Moving Granular Bed Filter, *Energy, Elsevier*, 2017, **120**, p 441–449
13. F. Wang, S. Hao, B. Dong, N. Ke, N.Z. Khan, L. Hao, L. Yin, X. Xu, and S. Agathopoulos, Porous-Foam Mullite-Bonded SiC-Ceramic Membranes for High-Efficiency High-Temperature Particulate Matter Capture, *J. Alloys Compd.*, 2022, **893**, p 162231
14. I.S. Hwang, J.-T. Park, and Y.L. Lee, Feasibility of a Porous Ceramic Filter for Collecting Brake Fine Dust, *Int. J. Automot. Technol.*, 2022, **23**(2), p 521–527
15. S. Li, H. Du, A. Guo, H. Xu, and D. Yang, Preparation of Self-Reinforcement of Porous Mullite Ceramics through in Situ Synthesis of Mullite Whisker in Flyash Body, *Ceram. Int.*, 2012, **38**(2), p 1027–1032
16. A. Barron, H. Scheinder, K. Okada, and J.A. Pask, Mullite and Mullite Ceramics, *Adv. Mater. Opt. Electron.*, 1995, **5**(5), p 284
17. H. Schneider, J. Schreuer, and B. Hildmann, Structure and Properties of Mullite-A Review, *J. Eur. Ceram. Soc.*, 2008, **28**(2), p 329–344
18. S. Pani, R.K. Sahoo, N. Dash, S.K. Singh, and B.K. Mohapatra, Cost Effective and Minimal Time Synthesis of Mullite from a Mine Waste by Thermal Plasma Process, *Adv. Mater. Lett.*, 2015, **6**(4), p 318–323
19. V. Viswabaskaran, F.D. Gnanam, and M. Balasubramanian, Mullitisation Behaviour of South Indian Clays, *Ceram. Int.*, 2002, **28**(5), p 557–564
20. J. Aguilar-Santillan, H. Balmori-Ramirez, and R.C. Bradt, Dense Mullite from Attrition Milled Kyanite and α-Alumina, *J. Ceram. Process. Res.*, 2007, **8**(1), p 1–11
21. L. Zhou, Z. Li, and Y. Zhu, Porous Silica/Mullite Ceramics Prepared by Foam-Gelcasting Using Silicon Kerf Waste as Raw Material, *Mater. Lett.*, 2019, **239**, p 67–70
22. R. Liu and D. Xiang, Recycling Photovoltaic Silicon Waste for Fabricating Porous Mullite Ceramics by Low-Temperature Reaction Sintering, *J. Eur. Ceram. Soc.*, 2021, **41**(12), p 5957–5966
23. A.N. Chen, J.Y. Chen, J.M. Wu, L.J. Cheng, R.Z. Liu, J. Liu, Y. Chen, C.H. Li, S.F. Wen, and Y.S. Shi, Porous Mullite Ceramics with Enhanced Mechanical Properties Prepared by SLS Using MnO_2 and Phenolic Resin Coated Double-Shell Powders, *Ceram. Int.*, 2019, **45**(17), p 21136–21143
24. C.O. Hulse and R.B. Graf, Effect of Temperature on the Mechanical Properties of Solid Pressure-Transmitting Media. II. Pyrophyllite, *J. Appl. Phys.*, 1965, **36**(5), p 1593–1596
25. T.K. Mukhopadhyay, S. Ghatak, and H.S. Maiti, Effect of Pyrophyllite on the Mullitization in Triaxial Porcelain System, *Ceram. Int.*, 2009, **35**(4), p 1493–1500
26. K.C. Rieger, Pyrophyllite, *Am. Ceram. Soc. Bull.*, 1992, **71**(5), p 500
27. R. Sule and I. Sigalas, Influence of Excess Alumina on Mullite Synthesized from Pyrophyllite by Spark Plasma Sintering, *Clay Miner.*, 2020, **55**(2), p 166–171
28. F. Wang, J. Ye, G. He, G. Liu, Z. Xie, and J. Li, Preparation and Characterization of Porous $MgAl_2O_4$ Spinel Ceramic Supports from Bauxite and Magnesite, *Ceram. Int.*, 2015, **41**(6), p 7374–7380
29. Z. Sun, J. Fan, and F. Yuan, Three-Dimensional Porous Silica Ceramics with Tailored Uniform Pores: Prepared by Inactive Spheres, *J. Eur. Ceram. Soc.*, 2015, **35**(13), p 3559–3566
30. S. Hashimoto, S. Honda, T. Hiramatsu, and Y. Iwamoto, Fabrication of Porous Spinel ($MgAl_2O_4$) from Porous Alumina Using a Template Method, *Ceram. Int.*, 2013, **39**(2), p 2077–2081
31. Z. Hou, H. Du, J. Liu, R. Hao, X. Dong, and M. Liu, Fabrication and Properties of Mullite Fiber Matrix Porous Ceramics by a TBA-Based Gel-Casting Process, *J. Eur. Ceram. Soc.*, 2013, **33**(4), p 717–725
32. R. Liu, J. Yuan, and W. Changan, A Novel Way to Fabricate Tubular Porous Mullite Membrane Supports by TBA-Based Freezing Casting Method, *J. Eur. Ceram. Soc.*, 2013, **33**(15–16), p 3249–3256
33. H. Guo, W. Li, and F. Ye, Low-Cost Porous Mullite Ceramic Membrane Supports Fabricated from Kyanite by Casting and Reaction Sintering, *Ceram. Int.*, 2016, **42**(4), p 4819–4826
34. A. Standard, C1424-15" Standard Test Method for Monotonic Compressive Strength of Advanced Ceramics at Ambient Temperature, *ASTM Int. West Conshohocken, PA, USA*, 2015
35. Y. Man, X. Luo, Z. Xie, D. Qu, and S. Jin, Influence of 3D Printed Topological Structure on Lightweight Mullite Load Bearing Board in Thermal Environment, *Adv. Mater. Sci. Eng.*, 2020, **2020**, p 1–8
36. J.A. Pask, Importance of Starting Materials on Reactions and Phase Equilibria in the Al_2O_3-SiO_2 System, *J. Eur. Ceram. Soc.*, 1996, **16**(2), p 101–108

37. D. Pereira, G.R.S. Biasibetti, R.V. Camerini, and A.S. Pereira, Sintering of Mullite by Different Methods, *Mater. Manuf. Process.*, 2014, **29**(4), p 391–396
38. K.C. Liu, G. Thomas, A. Caballero, J.S. Moya, and S. Deaza, Mullite Formation in Kaolinite-Alpha-Alumina, *Acta Metall. Mater.*, 1994, **42**(2), p 489–495
39. D. Pereira, G.R.S. Biasibetti, R.V. Camerini, and A.S. Pereira, Sintering of Mullite by Different Methods, *Mater. Manuf. Process.*, 2014, **29**, p 391–396
40. H.S. Tripathi, A. Ghosh, M.K. Halder, B. Mukherjee, and H.S. Maiti, Microstructure and Properties of Sintered Mullite Developed from Indian Bauxite, *Bull. Mater. Sci.*, 2012, **35**(4), p 639–643
41. R.L. Coble and W.D. Kingery, Effect of Porosity on Physical Properties of Sintered Alumina, *J. Am. Ceram. Soc.*, 1956, **39**(11), p 377–385
42. S. Meille and E.J. Garboczi, Linear Elastic Properties of 2D and 3D Models of Porous Materials Made from Elongated Objects, *Model. Simul. Mater. Sci. Eng.*, 2001, **9**(5), p 371–390
43. B.L. Metcalfe, The Synthesis, Microstructure and Physical Properties of High Purity Mullite, *Trans. J. Brit. Ceram. Soc.*, 1975, **74**, p 193–201
44. T. Huang, M.N. Rahaman, T. Mah, and T.A. Parthasarathay, Anisotropic Grain Growth and Microstructural Evolution of Dense Mullite above 1550 C, *J. Am. Ceram. Soc.*, 2000, **83**(1), p 204–210
45. S. Aramaki and R. Roy, Revised Phase Diagram for the System Al_2O_3-SiO_2, *J. Am. Ceram. Soc.*, 1962, **45**(5), p 229–242
46. A. Aksaf and J.A. Pask, Stable and Metastable Equilibria in the System SiO_2-Al_2O_3, *J. Am. Ceram. Soc.*, 1975, **58**(11–12), p 507–512
47. H. Guo and W. Li, Effects of Al_2O_3 Crystal Types on Morphologies, Formation Mechanisms of Mullite and Properties of Porous Mullite Ceramics Based on Kyanite, *J. Eur. Ceram. Soc.*, 2018, **38**(2), p 679–686
48. D. Goski, Reaction Sintering of Kyanite and Alumina to Form Mullite Composites, *Canad. Metall. Quart.*, 1999, **38**(2), p 119–126. https://doi.org/10.1016/S0008-4433(98)00041-X
49. D. Michel, L. Mazerolles, and R. Portier, Directional Solidification in the Alumina–Silica System Microstructures and Interfaces, *Mullite mullite matrix Compos.*, 1987, p 435–447
50. J. Ylä-Jääski and H.-U. Nissen, Investigation of Superstructures in Mullite by High Resolution Electron Microscopy and Electron Diffraction, *Phys. Chem. Miner.*, 1983, **10**(2), p 47–54
51. B. Dong, Z. Min, L. Guan, X. Zheng, L. Wang, Q. Wang, C. Yin, Y. Wang, R. Zhang, F. Wang, H. Abadikhah, X. Xin, Y. Zhang, and G. Wang, Porous Mullite-Bonded SiC Filters Prepared by Foaming-Sol-Gel-Tape Casting for High-Efficiency Hot Flue Gas Filtration, *Separat. Purificat. Technol.*, 2022, **295**, p 121338. https://doi.org/10.1016/j.seppur.2022.121338
52. J. Zheng and J.S. Reed, Particle and Granule Parameters Affecting Compaction Efficiency in Dry Pressing, *J. Am. Ceram. Soc.*, 1988, **71**(11), p C456–C458
53. R. Taktak, S. Baklouti, and J. Bouaziz, Effect of Binders on Microstructural and Mechanical Properties of Sintered Alumina, *Mater. Charact.*, 2011, **62**(9), p 912–916. https://doi.org/10.1016/j.matchar.2011.06.011
54. R. Zhang, C. Ye, X. Hou, S. Li, and B. Wang, Microstructure and Properties of Lightweight Fibrous Porous Mullite Ceramics Prepared by Vacuum Squeeze Moulding Technique, *Ceram. Int.*, 2016, **42**(13), p 14843–14848. https://doi.org/10.1016/j.ceramint.2016.06.118
55. D. Wu, J. Zhou, and Y. Li, Unbiased Estimation of Weibull Parameters with the Linear Regression Method, *J. Eur. Ceram. Soc.*, 2006, **26**(7), p 1099–1105. https://doi.org/10.1016/j.jeurceramsoc.2005.01.044
56. R. Bermejo, P. Supancic, and R. Danzer, Influence of Measurement Uncertainties on the Determination of the Weibull Distribution, *J. Eur. Ceram. Soc.*, 2012, **32**(2), p 251–255